PHYSICSAccess Research Paper
ISSN Online: 2756-3898, ISSN Print: 2714-500X https://doi.org/10.47514/phyaccess.2024.4.2.017

Enhanced Photovoltaic Features of Tin-doped Cobalt Molybdate Nanostructure Materials

Ijeh Rufus[1] and Imosobomeh L Ikhioya[2, 3]

[1] Department of Physics, University of Delta, Agbor, Delta State, Nigeria
[2] Department of Physics and Astronomy, University of Nigeria, Nsukka, 410001, Enugu State, Nigeria
[3] Department of Physics, Faculty of Science, Federal University Lokoja, Kogi State, Nigeria

Corresponding E-mail: rufus.ijeh@unidel.edu.ng

Received 25-10-2024
Accepted for publication 09-12-2024
Published 11-12-2024

Abstract

In this study, Sn-doped Cobalt molybdate was synthesized via an electrochemical deposition technique to enhance photovoltaic application. The Sn-doped CoMo has diffraction angles of (36.58°, 34.67°, 47.21°, 61.52°, 65.32°, 71.35°, and 75.67°), which correspond to the Miller indices (111, 211, 200, 211, 212, 300, and 311). Each peak, denotes a distinct crystal structure, indicating a polycrystalline material. A redshift indicates a smaller band gap, whereas a blueshift suggests a larger band gap. CoMo and Sn0.3@CoMo have low visible absorbance, whereas Sn0.1@CoMo and Sn0.2@CoMo have higher absorbance, making them better suited for photovoltaics, solar cells, photocatalysis, and energy storage applications. CoMo shows semiconductor qualities due to its 2.11 eV bandgap. The bandgap drop to 1.92 eV indicates that Sn caused extra energy levels in the bandgap. The FTIR spectrum of CoMo contains peaks related to metal-metal bonding and Mo-O vibrations. The bands between 600-800 cm^{-1} (Mo-O stretching) and 1000-200 cm^{-1} (Co-O stretching). Introducing Sn at a low concentration (0.1) causes modest changes or broadening of the existing peaks. The peaks at 300-400 cm^{-1} indicate Sn-O vibrations.

Keywords: Energy bandgap; semiconductor; cobalt molybdate; tin; photovoltaic.

I. INTRODUCTION

The population growth in developing nations has led to an increased demand for energy for a better lifestyle. The negative impact on human existence caused by environmental degradation and excessive carbon monoxide emissions is severe [1]–[4]. Acknowledging the importance of harnessing abundant sunlight, key technologies are recognized to address climate change. Therefore, researchers are exploring innovative materials for solar photovoltaic systems to replace traditional energy sources and meet the need for reliable, renewable, and clean energy [5]. These technologies focus on improving the efficiency of solar cells for better collection and conversion of sunlight into electrical power through photovoltaic systems [1]–[4], [6], [7]. Energy transformation and storage systems are crucial for a nation's sustainable economic strength. Developing practical electrical systems is vital for scientific and technological progress, specifically in producing cobalt molybdate-based electrode materials [8]. Thin film solar cells have found chalcogenides to be highly promising materials.

Cobalt molybdate (CoMo) exists in three polymorphs: α, β, and γ, each with a unique coordination of Mo6+ ions. The γ-phase occurs at elevated temperatures and pressures. Cobalt molybdate's electrical, optical, and catalytic properties entice researchers. This material has strong redox activity, photovoltaic, electrical conductivity, and catalytic properties. It has outstanding characteristics and can function as an electrode material [3], [6], [9]. The remarkable properties of

cobalt molybdate make it beneficial for various applications, such as oxygen production in chemical processes [10].

Reference [11] mentioned the effective ion radii of Tin (II) cation, which has six-fold ionic bonds ranging from 0.67 Å to 1.37 Å. This makes it useful for estimating nanocrystal structural characteristics. Tin's tiny ionic radius mixes with cobalt molybdate to increase surface area and intrinsic conductivity. Cobalt molybdate has been doped with manganese, chromium, nickel, iron, and gallium to improve energy storage performance in supercapacitors. [7]. Tin doping increases cobalt molybdate's conductivity, improving its effectiveness. Tin doping boosts thermal and chemical stability, resulting in longer-lasting materials. Fine-tuning a material's properties for applications is possible by adjusting the doping concentration. Despite extensive research on cobalt molybdate, the impact of tin doping is relatively unexplored, offering the potential for groundbreaking results. Sustainable material goals are advanced by developing new, less toxic, and more efficient materials.

This study will explore the photovoltaic applications of tin-doped cobalt molybdate through electrochemical techniques. Semiconductor. Doping aims to insert an intermediary level to lower the energy bandgap, enabling electron movement from the valence to the conduction band [12]. A highly efficient material is created through the collaborative action of dopant and host atom unpaired electrons. Studies on metal-doped cobalt molybdate have largely focused on its performance through potential sweeps, impedance spectroscopy, and charge-discharge cycles. We explored multiple approaches with a focus on photovoltaic applications. The decision stemmed from a lack of research into cost-effective and high-performance tin-doped cobalt molybdate thin films.

II. EXPERIMENTAL PROCEDURE

A. Preparation of FTO substrate

CoMo and Sn-doped CoMo were used to coat the FTO substrate. Approximately 2.5 cm^2 was the extent of the area covered by the FTO-immersed region. Before deposition, the FTO underwent a 15-minute cleaning process in ultrasonic baths with ethanol, acetone, distilled water, and ammonia water. The FTO was dried in an electric thermostatic oven at 65 °C for a predetermined period. FTO's large band gap allows it to be very transparent in the visible spectrum, making it ideal for solar cells and optoelectronic devices. A large concentration of free carriers from oxygen vacancies and fluorine doping increases the material's conductivity as a substrate, resulting in low electrical resistance. FTO's chemical stability makes it more durable and reliable in a variety of experimental circumstances than other conducting glasses.

B. Synthesis of CoMo and its Sn-doped variants

A solution with 0.1 M concentration and 10 mL volume is mixed with cobalt (II) nitrate hexahydrate $Co(NO_3)_2 \cdot 6H_2O$, sodium molybdate dihydrate $Na_2MoO_4.2H_2O$, and tin (II) sulfate $SnSO_4$ ranging from 0.1 to 0.3 mol in a 20/25 ml electrolyte solution. CoMo and Sn-doped CoMo were subjected to ECD analysis. The ECD setup, as shown in Fig. 1, comprises a DC power supply connected to a three-electrode cell. During every experiment at room temperature, the deposition remained constant for 15 seconds at a voltage of 10 V and pH of 5.4. The synthesized CoMo and Sn-doped CoMo were tested under controlled parameters. A 10 V potential was used for deposition in a 50-ml beaker with solvents. The electrochemical bath was established by adjusting the dopant molar concentrations from 0.1 to 0.3 mol. The bath system was filled with 10 ml of cobalt and molybdate precursor and 5 ml of Tin precursor. The material's tension dissipated when the resulting samples were heated to 200oC for 30 minutes. A Bruker D8-Advance X-ray diffractometer was used to analyze the structural properties of the films, with Cu-Kα radiation (ƛ = 1.5406 Å) in continuous-scan. The film's surface morphology was analyzed using MIRA3 TESCAN scanning electron microscopy. The 756S UV-visible spectrophotometer was used to conduct measurements of optical material wavelength ranging from 300 to 900 nm. The films' optical and solid-state properties were determined by analyzing the absorbance values using optical spectral analysis. Using the Jandel four-point probes method, we examined their electrical properties.

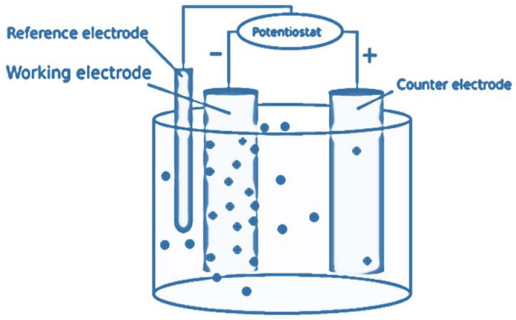

Fig. 1. Schematic diagram of electrochemical deposition technique (ECD).

III. RESULTS AND DISCUSSIONS

A. Structural study of cobalt molybdate and tin-doped cobalt molybdate

Fig. 2 shows the XRD diffraction patterns of CoMo, Sn0.1@CoMo, Sn0.2@CoMo, and Sn0.3@CoMo materials. The diffraction angles (26.56, 33.63, 37.31, 51.42, 61.52, 65.32, 71.35, and 75.67) correlate to certain crystal planes (011, 101, 111, 200, 211, 300, and 311). This depicts the material's atomic arrangement as well as its crystal structure. The intensity fluctuations at these angles disclose information about the density of the diffraction peaks, which helps to determine the crystal lattice's composition. The Sn-doped CoMo has diffraction angles of (36.58°, 34.67°, 47.21°, 61.52°, 65.32°, 71.35°, and 75.67°), which correspond to the Miller indices (111, 211, 200, 211, 212, 300, and 311). Each

peak, including numerous peaks, denotes a distinct crystal structure, indicating a polycrystalline material [5], [11]. The broadening of the peaks shows increased crystallite size (see Scherrer equation (1)). The peak intensities and locations are altered by adding tin (Sn) at various concentrations (0.1, 0.2, and 0.3), suggesting changes in crystallinity and phase composition. A slight alteration of the CoMo structure at low Sn concentration may improve photovoltaic and solar cell performance while preserving the crystal structure [9-12]. The moderate concentration induces more noticeable alterations, potentially resulting in higher peak intensities due to better crystallinity or the formation of new phases. When the concentration of Sn increases, the CoMo lattice undergoes phase segregation or distortion, which causes peak broadening or shifts in diffraction angles. The Scherrer equation (1) [13]–[23] was used to calculate the size of the crystallites by examining the width of the peaks. Sn inclusion alters lattice properties, indicating successful doping, the production of solid solutions, or even phase transitions. The crystallite size of the CoMo material is (4.77, 4.85, 4.90, 5.16, 5.41, 5.52, 5.72, and 5.89) nm, while the crystallite size of the Sn doped CoMo material is (2.44, 2.49, 2.53, 2.69, 2.75, 2.85, and 2.93) nm. A larger peak indicates lower crystallite size or higher microstrain as a result of Sn incorporation into the cobalt molybdate matrix.

$$D = \frac{k\lambda}{\beta Cos\theta} \quad (1)$$

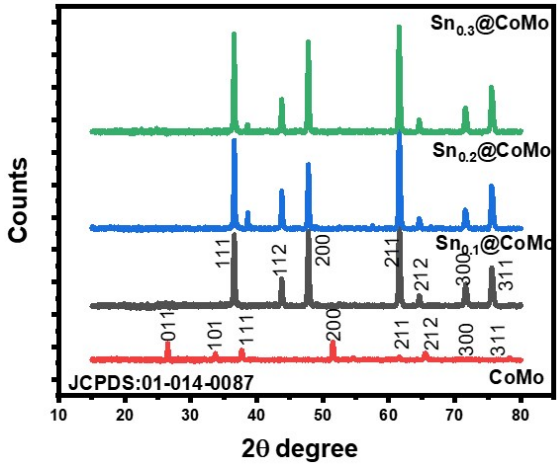

Fig. 2. XRD pattern of CoMo and its Sn-doped variants.

B. Optical study of Sn-doped CoMo

The UV-Vis spectrophotometry was used to quantify absorbance across several wavelengths, getting insights into the materials' electrical structure and illustrating how doping affects light absorption in Fig. 3. According to the Beer-Lambert Law, absorbance is proportional to the concentration of the absorbing substance. As Sn doping levels grow, so does absorbance, which affects the optical performance of the material. Fig. 3 (a) shows how the absorbance spectrum of cobalt molybdate (CoMo) and its Sn-doped derivatives changes with higher Sn concentration, resulting in increased light absorption. Despite this, the undoped cobalt molybdate (CoMo) outperforms the material doped with 0.3 mol Sn. These important modifications have a significant impact on solar and energy storage applications. The peak positions in the absorbance spectrum alter, indicating electronic transition shifts produced by Sn inclusion. A redshift indicates a smaller band gap, whereas a blueshift suggests a larger band gap. CoMo and Sn0.3@CoMo have low visible absorbance, whereas Sn0.1@CoMo and Sn0.2@CoMo have higher absorbance [4], [5], [10], making them better suited for photovoltaics, solar cells, photocatalysis, and energy storage applications. We can investigate how Sn concentration affects optical characteristics by doping at various levels (0.1, 0.2, and 0.3). The increase in visible range absorption suggests that photovoltaic, solar cell, photocatalysis, and energy storage applications could benefit from improved efficiency. The optical properties of CoMo and its Sn-doped versions change considerably as the Sn concentration increases. Optimizing materials is critical for many applications, particularly photonics and catalysis.

Fig. 3 (b) depicts the transmittance of CoMo, Sn0.1@CoMo, Sn0.2@CoMo, and Sn0.3@CoMo, providing information about their optical properties. These materials are more light-transmitting than absorbent. Each variation (0.1, 0.2, 0.3) represents a different Sn doping level, which influences the electrical structure and consequently transmittance behaviour. The transmittance of these materials is crucial for optoelectronics applications because increased optical properties lead to better performance in devices like sensors and solar cells. Cobalt molybdate's high transmittance implies excellent optical clarity, making it ideal for light transmission applications. Incorporating 0.1 Sn into CoMo changes its electrical structure, possibly affecting light transmission. When the Sn content is increased to 0.2%, the material's structure and electron mobility undergo significant changes. If transmittance continues to rise, it indicates that the doping levels have been tuned for better light transmission. Reduced transmittance implies that there is too much doping, resulting in more defects or scattered centres. When Sn concentrations approach 0.3, the material's optical properties are saturated [4], [5], [10]. A significant decrease in transmittance suggests increased light scattering or absorption due to material density or disorder. The measurement of transmittance in these materials is crucial for defining the best doping quantity and enhancing optical performance. Fig. 3(c) shows the reflectance of CoMo and its doped material, which include Sn0.1@CoMo, Sn0.2@CoMo, and Sn0.3@CoMo. The reflectance is increased by altering the Sn content, resulting in improved optical characteristics due to changes in electronic structure and surface interactions. The wavelength influences reflectance, revealing unique spectral features and material properties. The undoped reflectance levels are determined by the electrical structure and surface form. The undoped reflectance is used as a reference point to evaluate

how Sn doping changes optical characteristics. Incorporating 0.1 Sn lowered undoped reflectivity marginally. Changes in electrical band structure and surface roughness are responsible for this alteration. Reflectance changes more visibly after 0.2 Sn doping. The combination of Sn and CoMo produces various electronic states that affect light scattering and absorption. When the material's optical properties are properly regulated, its reflectance changes dramatically, potentially improving its performance in specific applications. Reflectance changes may occur at 0.3 Sn, possibly due to saturation effects or the development of new phases. Higher doping levels cause a rise in surface defects, which impair reflectivity. Increased reflectance enhances light control, whereas decreased reflectance disturbs the electrical structure due to excess Sn.

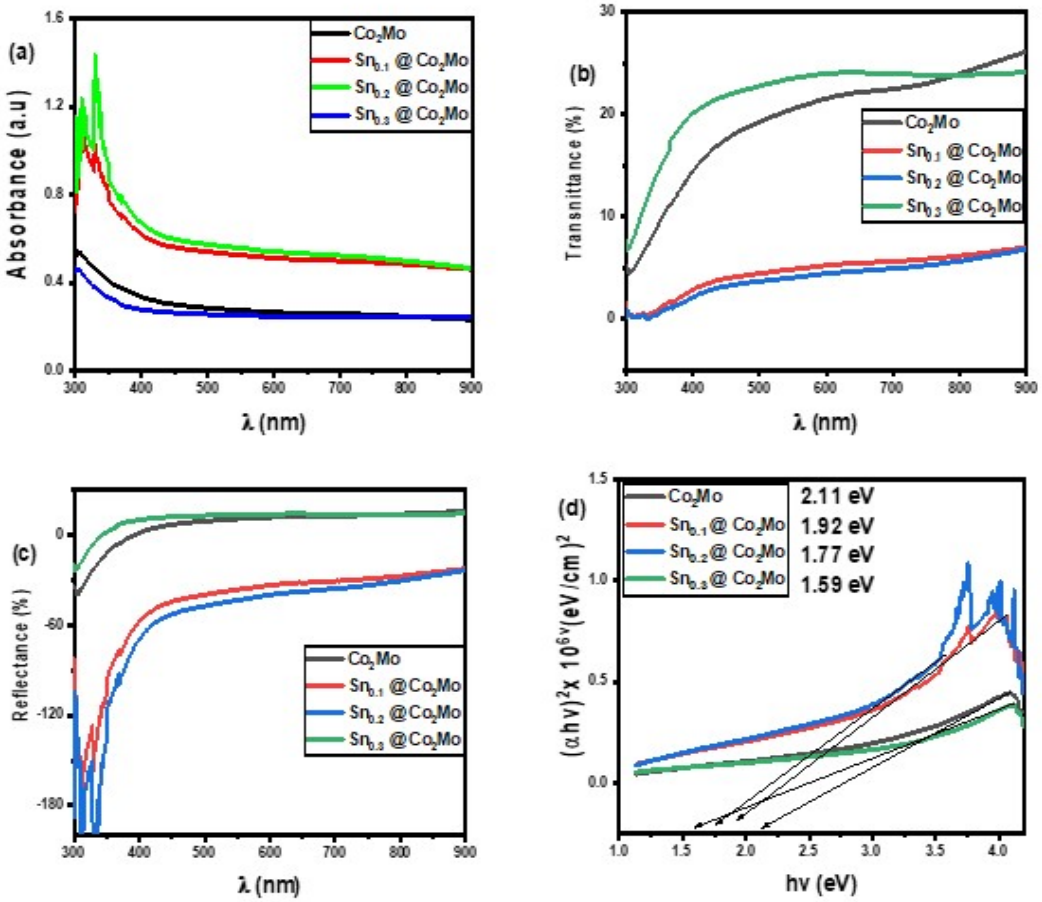

Fig. 3. (a) Absorbance, (b) transmittance, (c) reflectance, and (d) bandgap energy of undoped and Sn-doped material.

In Fig. 3 (d), the energy bandgap values of CoMo and Sn-doped CoMo indicate how Sn affects the material's electronic properties, with lower bandgap values indicating increased conductivity or changes in semiconductor behaviour. CoMo's bandgap decreases as Sn doping concentrations increase. Doping with Sn alters the electrical structure by adding new energy levels to the bandgap. This change improves charge carrier mobility and has ramifications for the material's prospective use in electronics and photonics. Increasing Sn concentrations reduces bandgap energy from 2.11 eV to 1.59 eV, improving the performance of devices with lower energy barriers, such as transistors and solar cells. CoMo shows semiconductor qualities due to its 2.11 eV bandgap. To pass from the valence band to the conduction band, an electron requires 2.11 eV of energy [4], [5], [10]. The bandgap drop to 1.92 eV indicates that the presence of Sn caused extra energy levels in the bandgap. The reduction in bandgap to 1.77 eV implies that the material is more conductive. The reduction in bandgap to 1.59 eV indicates significant changes in the electrical structure.

C. FTIR study of cobalt molybdate and tin-doped cobalt molybdate

Fig. 4 illustrates how FTIR analysis reveals functional groups and bonds in CoMo and Sn-doped versions by examining absorption peaks in the spectrum. Each shift in the peak correlates to distinct chemical conditions or doping-induced changes. Doping CoMo with Sn improves the

material's photovoltaic activity by altering electronic characteristics and stability, as seen in FTIR spectra via changes in bond vibrations. The FTIR spectra for variants 0.1, 0.2, and 0.3@CoMo exhibit gradual modifications, demonstrating a relationship between dopant concentration and structural/chemical changes in the materials. The FTIR spectrum of CoMo contains peaks related to metal-metal bonding and Mo-O vibrations [3], [5], [6], [10]. The bands between 600-800 cm^{-1} (Mo-O stretching) and 1000-1200 cm^{-1} (Co-O stretching). The introduction of Sn at a low concentration (0.1) causes modest changes or broadening of the existing peaks. The peaks at 300-400 cm^{-1} indicate Sn-O vibrations. The alterations indicate that Sn interacts with the CoMo matrix, potentially increasing photovoltaic activity by modifying electrical characteristics. At 0.2 Sn concentration, more dramatic changes and peaks emerge. The Sn-O associated peaks become increasingly intense, indicating more Sn incorporation into the lattice. This suggests a greater connection between Sn and CoMo, which enhances photovoltaic performance and stability. At 0.3 Sn concentration, the FTIR spectrum changes significantly, with new peaks and the removal of several CoMo peaks. Sn-O vibrations dominate the spectrum, indicating significant Sn incorporation. This shows that extensive Sn doping promotes the creation of new phases. As the Sn concentration increases, the FTIR spectra show changes in the bonding environment, demonstrating that Sn is successfully changing the CoMo structure. The observed spectrum changes are consistent with projected increases in photovoltaic activity due to improved electron transport and stability.

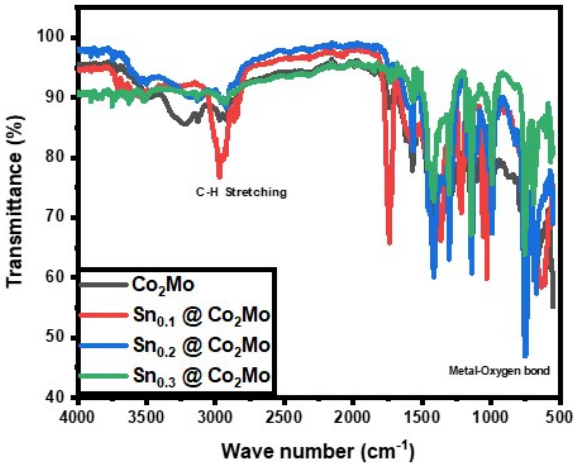

Fig. 4. FTIR of CoMo and its Sn-doped variants.

D. Surface microstructures of CoMo, Sn0.1@CoMo, Sn0.2@CoMo, and Sn0.3@CoMo.

Fig. 5 shows that the microstructures of CoMo, Sn0.1@CoMo, Sn0.2@CoMo, and Sn0.3@CoMo each have distinct properties determined by doping levels and element interactions. CoMo's grain structure is distinct and distinctive.

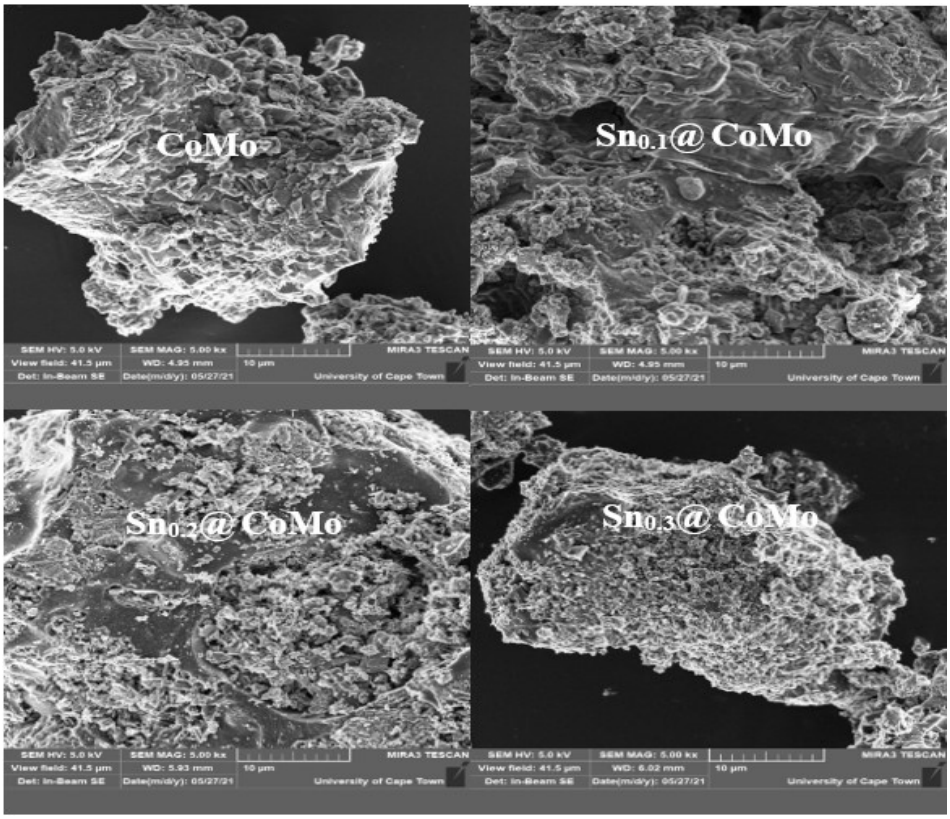

Fig. 5. SEM of CoMo and its Sn-doped variants.

The size and distribution of grains have an impact on photovoltaic and solar cells, impacting their performance and stability. Moderate surface aggregation influences the adsorption characteristics of reactions. The addition of 0.1 mol Sn to the CoMo lattice alters the surface morphology, resulting in smaller particle sizes. The incorporating 0.2 mol Sn results in a surface with more distinguishing properties, such as increased porosity or different phases [3], [5], [6], [10]. The shape enhanced the performance of photovoltaic and solar cells by expanding the active area. Sn creates a more equally dispersed surface than other doping levels. When 0.3 mol of Sn is introduced, the morphology varies considerably in comparison to CoMo, with aggregation or phase separation. The surface's complexity grows as critical elements influence its performance. Surface morphological alterations have a direct impact on photovoltaic and solar cell activity, with optimal doping levels improving performance and excessive doping reducing it.

Fig. 6 and Table I show how EDX is used to perform elemental analysis and calculate the composition of CoMo and its derivatives. Measuring the substance indicates the relative amounts of each ingredient. Sn content variations affect the electrical and structural properties of Sn0.1@CoMo, Sn0.2@CoMo, and Sn0.3@CoMo.

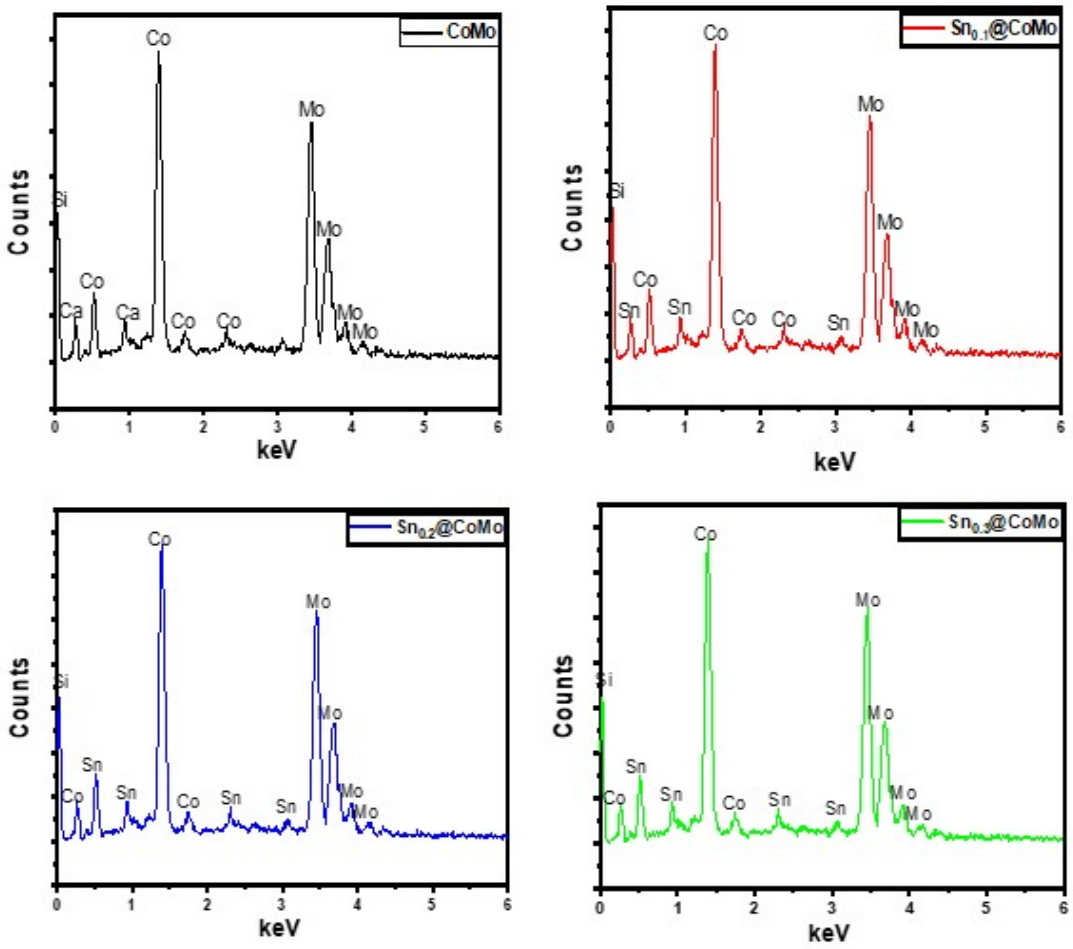

Fig. 6. EDX of CoMo and its Sn-doped variants.

Table I. EDX spectra atomic weight percentages of the constituent elements.

CoMo Component	Atomic Weight (%)	Sn0.1@CoMo Component	Atomic Weight (%)	Sn0.2@CoMo Component	Atomic Weight (%)	Sn0.3@CoMo	
Co	60.00	Co	59.00	Co	59.00	Co	58.00
Mo	37.0	Mo	37.00	Mo	36.00	Mo	36.00
Ca	0.90	Ca	0.90	Ca	0.90	Ca	0.90
Si	2.10	Sn	1.00	Sn	2.00	Sn	3.00
-	-	Si	2.10	Si	2.10	Si	2.10

The EDX analysis indicated variances in CoMo elemental ratios with Sn ranging from 0.1 to 0.3, which have an impact on photovoltaic and solar cell performance, as well as electrical properties. The various peaks in each version represent Sn and CoMo components. The primary elements detected were cobalt (Co) and molybdenum (Mo). The EDX spectrum shows separate peaks corresponding to various components. The Co/Mo ratio exposes the features of the material's photovoltaic and solar cells. The addition of 0.1 atomic percent Sn resulted in the appearance of additional peaks in the EDX spectrum, which correspond to tin. At this low concentration, Sn changes the electrical characteristics and increases the surface area, potentially increasing the activity of photovoltaic and solar cells while not appreciably affecting the Co and Mo ratios. The Sn peaks in the EDX spectrum are stronger at 0.2 Sn than Sn0.1@CoMo. Increasing the concentration improves the material's characteristics, resulting in increased stability and selectivity in reactions. The interaction between Sn and CoMo has a substantial impact on the electrical structure. The addition of Sn beyond 0.3 reduces the activity of photovoltaic and solar cells, potentially due to agglomeration or phase separation. The correct balance of Co, Mo, and Sn is critical, as too much Sn obstructs the important active areas for photovoltaic and solar cells. As Sn concentration increases, so does the strength of Sn peaks in the EDX spectrum, indicating successful absorption into the CoMo structure.

E. Electrical study of CoMo and its Sn-doped variants

Using the relations [24]–[38], the resistivity and conductivity of the CoMo and its Sn-doped variants were determined.

$$R_s = R\left({}^{V}/_{I}\right) \quad (2)$$

Where $K = {}^{\pi}/_{ln2}$

$$\rho = t \times R_s \quad (3)$$

$$\sigma = {}^{1}/_{\rho} \quad (4)$$

Table II displays the resistivity and conductivity of CoMo and Sn-doped CoMo at various dopant concentrations. The materials' thickness decreased from 121.24 to 106.12 nm, and the film resistivity decreased from 9.34 to 2.62 Ω.m. Conductivity decreased from 5.79 to 2.22 S/m. The deposition of materials involved dopant molarities ranging from 0.1 to 0.3 mol. The films produced are suitable for photovoltaic and solar applications due to their high resistivity and low conductivity.

Table II. Electrical properties of CoMo and its Sn-doped variants.

Specimen	T (nm)	ρ $(\Omega m) \times 10^{-8}$	σ $(S/m) \times 10^{7}$
CoMo	121.24	9.34	5.79
$Sn_{0.1}$@CoMo	118.06	7.92	1.54
$Sn_{0.2}$@CoMo	111.02	5.84	1.35
$Sn_{0.3}$@CoMo	106.12	2.62	2.22

IV. CONCLUSION

We have successfully synthesized cobalt molybdate and tin-doped cobalt molybdate via electrochemical deposition technique. The crystallite size of the CoMo material is (4.77, 4.85, 4.90, 5.16, 5.41, 5.52, 5.72, and 5.89) nm, while the crystallite size of the Sn doped CoMo material is (2.44, 2.49, 2.53, 2.69, 2.75, 2.85, and 2.93) nm. A larger peak indicates lower crystallite size or higher micro-strain as a result of Sn incorporation into the cobalt molybdate matrix. The materials' thickness decreases from 121.24 to 106.12 nm, and the film resistivity decreases from 9.34 to 2.62 Ωm. Consequently, conductivity decreased from 5.79 to 2.22 S/m. The addition of 0.1 mol Sn to the CoMo lattice alters the surface morphology, resulting in smaller particle sizes. The addition of Sn increases surface area, hence improving photovoltaic and solar cell performance. The FTIR spectra for variants 0.1, 0.2, and 0.3@CoMo exhibit gradual modifications, demonstrating a relationship between dopant concentration and structural/chemical changes in the materials. The FTIR spectrum of CoMo contains peaks related to metal-metal bonding and Mo-O vibrations. The bands between 600-800 cm^{-1} (Mo-O stretching) and 1000-1200 cm^{-1} (Co-O stretching). The introduction of Sn at a low concentration (0.1) causes modest changes or broadening of the existing peaks. The peaks at 300-400 cm^{-1} indicate Sn-O vibrations. CoMo shows semiconductor qualities due to its 2.11 eV bandgap. The bandgap drop to 1.92 eV indicates that the presence of Sn caused extra energy levels in the bandgap. The ionic radius of Sn^{2+} (around 0.69 Å) is smaller than that of Co^{2+} (roughly 0.74 Å) and Mo^{6+} (approximately 0.62 Å). This size mismatch caused substantial lattice distortions in the crystal structure when Sn substituted Co or Mo. Introducing a smaller Sn ion causes local lattice distortions, altering bond lengths and angles. This distortion interrupts the crystal structure's regular pattern, affecting the material's stability. Vacancies or interstitial defects, caused by distortion, affect the material's electronic properties. Conductivity is affected by these defects, which act as charge carriers or traps. Although better charge carrier mobility usually improves conductivity, the defects from distortion also affect conductivity. Defects create extra routes for charge movement. Complex conductivity arises from the combined effects of doping-induced carrier concentration and lattice distortion scattering.

ACKNOWLEDGEMENT

The valuable contributions of the authors were key to the success of the research.

References

[1] M. C. Liu, L. Kong, L. C. Bin, X. M. Li, Y. C. Luo, and L. Kang, "Facile fabrication of $CoMoO_4$ nanorods as electrode material for electrochemical capacitors". Mat. Lett., vol. 94, pp. 197–200, 2013. https://doi.org/10.1016/j.matlet.2012.12.057.

[2] W. J. Li, R. Y. Fan, X. J. Tian, J. L. Tan, J. Y. Lv, N. Yu, B. Liu, Y. M. Chai, and B. Dong, "Ultralow-Pt-loading assisted by reconstruction of cobalt molybdate nanoarrays for enhanced hydrogen evolution reaction". Int. J. of H. Energy, vol. 56, pp. 837–843, 2024. https://doi.org/10.1016/j.ijhydene.2023.12.253.

[3] W. Li, X. Wang, Y. Hu, L. Sun, C. Gao, C. Zhang, H. Liu and M. Duan, "Hydrothermal synthesized of comoo4 microspheres as excellent electrode material for supercapacitor". Nanoscale Res. Lett., vol. 13, no. 1, 2018. https://doi.org/10.1186/s11671-018-2540-3.

[4] M. Edrissi, S. Samadanian-Isfahani, and M. Soleymani, "Preparation of cobalt molybdate nanoparticles; Taguchi optimization and photocatalytic oxidation of Reactive Black 8 dye," Powder Tech.., vol. 249, pp. 378–385, 2013, doi: 10.1016/j.powtec.2013.08.022.

[5] D. O. Obada, M. Muhammad, S. B. Tajiri, M. O. Kekung, S. A. Abolade, S. B. Akinpelu, and A. Akande, "A review of renewable energy resources in Nigeria for climate change mitigation". Case Stud. in Chem. & Env. Eng., vol. 9, 2024. https://doi.org/10.1016/j.cscee.2024.100669.

[6] Y. Zhang, L. Li, H. Su, W. Huang and X. Dong, "Binary metal oxide: Advanced energy storage materials in supercapacitors". J. of Mat. Chem. A vol. 3, no. 1, pp. 43–59, 2015. https://doi.org/10.1039/c4ta04996a.

[7] X. Zhang, L. Yue, S. Zhang, Y. Feng, L. An, M. Wang and J. Mi, J. "Nickel-doped cobalt molybdate nanorods with excellent cycle stability for aqueous asymmetric supercapacitor". Int. J. of H. Energy, vol. 45, no. 15, pp. 8853–8865, 2020. https://doi.org/10.1016/j.ijhydene.2020.01.127.

[8] F. Samimi, M. Ghiyasiyan-Arani, M. A. Mahdi, L. S. Jasim, A. F. Zonouz and M. Salavati-Niasari, "Preparation, microstructural characteristics, and electrochemical properties of cobalt molybdate nanocomposites as electrode material for hydrogen storage". J. of Energy Storage, vol. 85, 2024. https://doi.org/10.1016/j.est.2024.111027.

[9] I. S. Altarawneh, S. E. Rawadieh, M. A. Batiha, L. A., Al-Makhadmeh, M. A., Al-Shaweesh and M. K. Altarawneh, "Structures and thermodynamic stability of cobalt molybdenum oxide ($CoMoO_4$-II). Surf. Sci., vol. 677, pp. 52–59, 2018. https://doi.org/10.1016/j.susc.2018.05.018.

[10] M. Zang, N. Xu, G. Cao, Z. Chen, J. Cui, L. Gan, H. Dai, X., Yang and P. Wang, "Cobalt Molybdenum Oxide Derived High-Performance Electrocatalyst for the Hydrogen Evolution Reaction". ACS Catalysis, vol. 8, no. 6, pp. 5062–5069, 2018. https://doi.org/10.1021/acscatal.8b00949.

[11] V. Sidey V, "On the effective ionic radii for the tin(II) cation". J. of Phy. Chem. Solids, vol. 171, 2022, doi: 10.1016/j.jpcs.2022.110992.

[12] R. O. Ijeh, A. C. Nwanya, A. C., Nkele, I. G. Madiba, A. K. H. Bashir, A. B. C. Ekwealor, R. U. Osuji, M. Maaza and F. Ezema, "Optical, electrical and magnetic properties of copper doped electrodeposited MoO_3 thin films". Ceramics Int., vol. 46, no. 8, pp. 10820–10828, 2020. https://doi.org/10.1016/j.ceramint.2020.01.093.

[13] K. I. Udofia, I. L. Ikhioya, D. N. Okoli and A. J. Ekpunobi and "Impact of doping on the physical properties of PbSe chalcogenide material for photovoltaic application". Asian J. of Nanosci. & Mat., vol. 6, no. 2, pp. 135–147, 2023. https://doi.org/10.26655/AJNANOMAT.2023.2.3.

[14] K. I. Udofia, I. L. Ikhioya, A. U. Agobi, D. N. Okoli and A. J. Ekpunobi, "Effects of zirconium on electrochemically synthesized tin selenide materials on fluorine-doped tin oxide substrate for photovoltaic application. Journal of the Indian Chemical Society, vol. 99, no, 10, pp. 100737, 2022. https://doi.org/10.1016/j.jics.2022.100737.

[15] S. Afzal, S. Tehreem, T. Munir, S. G. Sarwar and I. L. Ikhioya, "Impact of Transition Metal Doped Bismuth Oxide Nanocomposites on the Bandgap Energy for Photoanode Application". J. of Nano & Mat. Sci. Res. vol. 2, no. 1, pp. 104–109, 2023.

[16] E. N. Josephine, O. S. Ikponmwosa and I. L. Ikhioya, "Synthesis of SnS/SnO Nanostructure material for Photovoltaic Application," East Eur. J. of Phy., vol. 2023, no. 1, pp. 154–161, 2023. doi: 10.26565/2312-4334-2023-1-19.

[17] E. N. Josephine, O. S. Ikponmwosa and I. L. Ikhioya, "Enhanced physical properties of SnS / SnO semiconductor material," Asian J. of Nanosci., vol. 3, pp. 199–212, 2023, doi: 10.26655/AJNANOMAT.2023.3.3.

[18] I. L. Ikhioya, N. I. Akpu, E. U. Onoh, S. O. Aisida, I. Ahmad, M. Maaza and F. Ifeanyichukwu, "Impact of precursor temperature on physical properties of molybdenum doped nickel telluride metal chalcogenide material". Asian J. of Nanosci., vol. 2, pp. 156–167, 2023, doi: 10.26655/AJNANOMAT.2023.2.5.

[19] I. L. Ikhioya, C. O. Ugwuoke, F. U. Ochai-ejeh, I. L. Ikhioya, C. O. Ugwuoke and F. U. Ochai-ejeh, "Optimisation of temperature regulator on spray pyrolysis cobalt selenide doped erbium (CoSe : Er) semiconductor material for photovoltaic application". Mat. Res. Innov., vol. 00, no. 00, pp. 1–8, 2023. https://doi.org/10.1080/14328917.2023.2213493.

[20] I. L. Ikhioya, C. O. Ugwuoke, D. N. Okoli, A. J. Ekpunobi, M. Maaza, and F. I. Ezema, "Effect of cobalt on the photovoltaic properties of zinc selenide thin film deposited on fluorine-doped tin oxide (FTO) via electrochemical deposition technique," Curr. Res. Green Sustain. Chem., vol. 5, no. 05, pp. 100328, 2022. doi: 10.1016/j.crgsc.2022.100328.

[21] I. L. Ikhioya, G. M. Whyte and A. C. Nkele, "Temperature-modulated nanostructures of ytterbium-doped Cobalt Selenide (Yb-CoSe) for photovoltaic applications". J. of the Indian Chem. Soc., vol. 100, no. 1, pp. 100848, 2023. https://doi.org/10.1016/j.jics.2022.100848.

[22] Emmanuel, O. C., Donald, O. N., & L. Ikhioya, I. (2022). Effect of Doping and Co-sensitization on the Photovoltaic Properties of Natural Dye-sensitized Solar Cells. International Journal of Applied Physics, 9(3), 44–54. https://doi.org/10.14445/23500301/ijap-v9i3p105.

[23] J. Damisa, J. O. Emegha, and I. L. Ikhioya, "Deposition Time induced Structural and Optical Properties of Lead Tin Sulphide Thin Films". J. of the Nig. Soc. of Phy. Sci., vol. 3, no. 4, pp. 455–458, 2021. https://doi.org/10.46481/jnsps.2021.157.

[24] A. I. Agbrara, E. O. Ojegu, M. O. Osiele, and I. L. Ikhioya, "Electrochemically Synthesize SrSe/ZrSe Heterostructure Material for Photovoltaic Application". Adv. J. of Chem., Section A, vol. 6, no. 4, pp. 401–411, 2023. https://doi.org/10.48309/AJCA.2023.407032.1385.

[25] N. Akpu, U. Okpechi, N. Elizabeth, I. Imosobomeh, O. Julian, L. Nnanna, and I. Agbodike, "Impact of temperature difference on the features of spray deposited yttrium doped cobalt selenide (YCoSe) thin films for photovoltaic application". African Sci. Rep., vol. 2, no. 143, 2023. https://doi.org/10.46481/asr.2023.2.3.143.

[26] S. O. Malumi, T. Malumi, M. O. Osiele, and I. L. Ikhioya, "Enhance and Performance Evolution of Silver-Doped Titanium Dioxide Dye-Sensitized Solar Cells Using Different Dyes". J. of Eng. & Ind. Res., vol. 4, no. 4, pp. 189–200, 2023.

[27] S. O. Samuel, M. L. E. Frank, E. P. Ogherohwo, A. Ekpekpo, J. T. Zhimwang, and I. L. Ikhioya, "Influence of Deposition Voltage on Strontium Sulphide Doped Silver for Optoelectronic Application". East Euro. J. of Phy., vol. 2023, no. 1, pp. 189–196, 2024. https://doi.org/10.26565/2312-4334-2023-1-25.

[28] I. Rufus and I. L. Ikhioya, "Enhanced electrical, morphology, structural, and optical features of nickel silver sulphide material". J. of Basic Phy. Sci., vol. 11, no. 2, pp. 1–9, 2023.

[29] H. Shah, S. Afzal, M. Usman, K. Shahzad, and I. L. Ikhioya, "Impact of Annealing Temperature on Lanthanum Erbium Telluride (La0.1Er0.2Te0.2) Nanoparticles Synthesized via Hydrothermal Approach". Adv. J. of Chem., Sect. A vol. 6, no. 4, pp. 342–351, 2023. https://doi.org/10.22034/AJCA.2023.407424.1386.

[30] C. Uchechukwu, A. Osita, J. Chukwuemeka, I. Lucky, and O. Odira, "Investigating the influence of natural dye extracts from Ocimum gratissimum, Solanum melongena, Piper guineese, and their blend in the fabrication of perovskite solar cells," Hybrid Adv., vol. 6, 04, pp. 100198, 2024, doi: 10.1016/j.hybadv.2024.100198.

[31] L. I. Ikhioya, N. I. Akpu, and F. U. Ochai-Ejeh, "Influence of erbium (Er) dopant on the enhanced optical properties of electrochemically deposited zinc oxide (ZnO) films for high-performance photovoltaic systems". Optik (Stuttg)., vol. 252, no. December 2021, p. 168486, 2022, doi: 10.1016/j.ijleo.2021.168486.

[32] L. I. Ikhioya, S. O. Aisida, I. Ahmad and F. I. Ezema, "The effect of molybdenum dopant on rare earth metal chalcogenide material". Chem. Phy. Impact, vol. 7, 2023, doi: 10.1016/j.chphi.2023.100269.

[33] L. I. Ikhioya, N. I. Akpu, and A. C. Nkele, "Influence of ytterbium (Yb) dopant on the optical properties of electrochemically deposited zinc oxide (ZnO) films". Mat. Res. Exp., vol. 8, no. 1, 2021, doi: 10.1088/2053-1591/abd5d6.

[34] A. Hussain., S. Habib, I. Ullah, F. Sahreen, I. Ahmad and I. Ikhioya, "Enhanced Structural, Morphological and Optical Features of Tix MnNiO (X= 1, 2, and 3 mL) Synthesized Using Hydrothermal Approach. Eurasian J. of Sci. & Tech., vol. 4, no. 3, pp. 195-207, 2024. doi: 10.48309/ejst.2024.428429.1117.

[35] L. I. Ikhioya and A. C. Nkele, "Green synthesis and characterization of aluminium oxide nanoparticle using neem leaf extract (Azadirachta Indica)". Hybrid Adv., vol. 5, no. November 2023, p. 100141, 2024, doi: 10.1016/j.hybadv.2024.100141.

[36] L. I. Ikhioya, O. B. Uyoyou and A. L. Oghenerivwe, "The effect of molybdenum-doped tin selenide semiconductor material (SnSe) synthesized via electrochemical deposition technique for photovoltaic application". J. Mat. Sci. Mater. Electron., vol. 33, no. 13, pp. 10379–10387, 2022, doi: 10.1007/s10854-022-08025-y.

[37] E. O. Ojegu, S. O. Samuel, M. O. Osiele, G. E. Akpojotor, and I. L. Ikhioya, "Optimisation of deposition voltage of zirconium-doped chromium telluride via typical three-electrode cell electrochemical deposition technique". Mat. Res. Innov., vol. 00, no. 00, pp. 1–9. 2023. https://doi.org/10.1080/14328917.2023.2243063.

[38] I. O. Blessing, H. Shah, S. Afzal, and I. L. Ikhioya, "Enhanced structural properties of electrochemically synthesised NiFeS using 500 keV carbon C++ ions irradiation," Mat. Res. Innov., vol. 28, no. 4, pp. 251–262. https://doi.org/10.1080/14328917.2023.2262315.